PHOTONICS Research

Intelligent all-fiber device: storage and logic computing

Zhihai Liu,[1,2] Siying Cheng,[1] Yu Zhang,[1,*] Wei Jin,[1] Xiang Li,[1] Yaru Li,[1] Yaxun Zhang,[1,4] Xinghua Yang,[1] Jianzhong Zhang,[1] and Libo Yuan[3]

[1]Key Laboratory of In-fiber Integrated Optics, Ministry of Education, Harbin Engineering University, Harbin 150001, China
[2]National Demonstration Center for Experimental Physics Education, Harbin Engineering University, Harbin 150001, China
[3]Photonics Research Center, Guilin University of Electronics Technology, Guilin 541004, China
[4]e-mail: zhangyaxun@hrbeu.edu.cn
*Corresponding author: zhangy0673@163.com

Received 4 August 2021; revised 15 November 2021; accepted 5 December 2021; posted 7 December 2021 (Doc. ID 439506); published 14 January 2022

The typical functions of the optical fiber are communication and sensing. However, the fiber functions need to extend to meet the requirements of the development of artificial intelligence. This paper achieves an all-fiber device with storage and logic computing functions using a single-mode fiber and $Ge_2Sb_2Te_5$ (GST) material. We use the pulse amplitude modulation (the switching energy is about 50 nJ) to switch the GST state for performing the eight-level data storage (3-bit). The all-fiber memory device has the advantages of high optical contrast (about 38%), good reversibility, and high repeatability. We implement the all-optical logic operations ("AND" and "OR") by using two memory cells in series and parallel. For the first time, we use the single-mode optical fiber to realize storage and computing functions, and this intelligent fiber has tremendous application potential in intelligent optical fiber communication and portends a new paradigm for brain-like computing.

https://doi.org/10.1364/PRJ.439506

1. INTRODUCTION

In the era of fifth-generation (5G) mobile communication [1–3], optical fiber continues to play an essential role due to superfast transmission speed, tremendous bandwidth, and multiplexing capability in terms of wavelength [4]. With the rapid development of high-speed bandwidth services, higher requirements have been put forward for the optical fiber and transmission network's functions, flexibility, and expansibility [5–7]. It requires the intelligent transformation in optical communication while realizing the large-capacity and ultra-high-speed transmission [8]. Therefore, we try to entrust optical fiber novel functions, storage, and computing, to serve intelligent optical communication more competently in addition to what we know about optical transmission function.

The common approaches to achieving light storage rely on either the bistability of artificial optical resonances [9–15] or the inherent bistable characteristics of devices stemming from their material properties [16–20]. These optical memories mainly rely on the master–slave configuration [9–12], the feedback loop scheme [13–15], or the injection-locking techniques [16–20], which have high integration density, short memory access time, and low-energy consumption. However, these devices are complex and volatile (extra energy is required to maintain the state of memory). Phase-change materials (PCMs) are ideal candidates for nonvolatile memories, which have large contrast in electrical/optical properties between the crystalline state and the amorphous state. They have been extensively studied and applied for electronic memories [21–26]. However, the "electronic rate bottleneck" of electronic memories limits modern computing technology development. All-optical memory based on PCMs can mitigate the von Neumann bottleneck with high speed and low power consumption in data transmission. The researchers use In_3SbTe_2 [27], $CsPbIBr_2$ [28], $Ge_2Sb_2Te_5$ (GST) [29–32], $Ge_2Sb_2Se_4Te$ [33], $Ag_5In_5Sb_{60}Te_{30}$ [34,35], and other PCMs to achieve optical memories; in particular, the GST has the best performance in terms of speed and stability. Reference [30] demonstrates a fast nonvolatile GST-based PCM memory with a capacity of 3 bits, occupying an area of only 0.4 μm × 0.4 μm, and the speed was close to 1 GHz. The recent GST memory realized the 12-level all-optical storage and realized logic operations (logic "OR" and "NAND") by using the pulse-width modulation method [36]. However, current chip-to-fiber coupling relies on edge or grating couplers with limitations in alignment tolerances, efficiency, and bandwidth, respectively [37], so the waveguide-based device is difficult to make compatible with

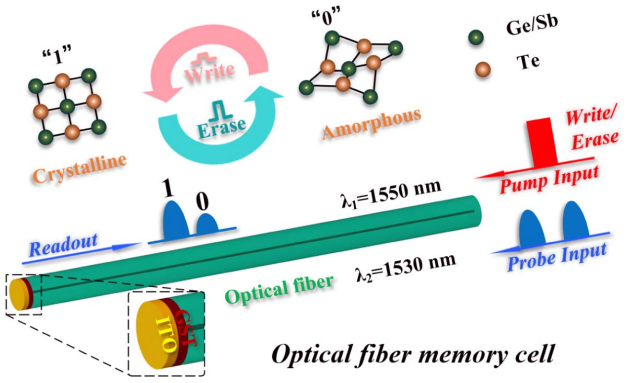

Fig. 1. Operation principle of the all-fiber memory device. The fiber memory cell consists of fiber, GST, and ITO (as the capping layer). The information is stored in the phase state of GST and encoded as the GST's reflectivity (amorphous state: logic state 0, low-reflectivity state; crystalline state: logic state 1, high-reflectivity state). Pump pulse ($\lambda_1 = 1550$ nm) and probe light ($\lambda_2 = 1530$ nm) into the optical fiber storage unit to write/erase and read the information.

optical fiber communication systems. We design a PCMs-based all-fiber memory, which can couple light to and from optical fiber communication network with large efficiency.

Herein, we demonstrate all-fiber memory by combining the ordinary single-mode optical fiber (Corning SMF-28), GST, and indium-tin-oxide (ITO) (as the capping layer). Since GST has a significant contrast in optical reflectivity between the amorphous state (logic state 0, low-reflectivity state) and the crystalline state (logic state 1, high-reflectivity state), information is encoded as the reflectivity of the GST. It is stored in the phase state of GST. We use pump pulse ($\lambda_1 = 1550$ nm) with a fixed pulse width to switch the state of GST (the low-energy pulse converts GST to the crystal state, and the high-energy pulse converts GST to the amorphous state), and the switching energy of the all-fiber memory is as low as about 50 nJ. We use continuous light ($\lambda_2 = 1530$ nm) whose energy is much lower (0.2 mW) than the switching energy to achieve data reading. The operation principle of the all-optical fiber memory is shown in Fig. 1. We perform eight-level storage (3-bit) with high repeatability and excellent reversibility using the pulse amplitude modulation (PAM) method, and the optical contrast is about 38%. Moreover, each memory level has an associated PAM parameter that will always result in written memory level, whatever the starting state. We further explore its application to the provision of a nonvolatile logical fiber calculator, achieving "AND" and "OR" computations. The presented all-fiber memory opens new routes toward the intelligent fiber system [38].

2. PRINCIPLE

GST is a kind of chalcogenide phase-change material. It has a wide range of applications in near-infrared absorbers and modulators [39], data storage [40], and data calculation [41,42]. GST has two phases corresponding to the amorphous structure (a-GST) and cubic structure (c-GST). The two phases have very different material properties, thus providing the contrast requirements of distinguished logical states [43]. The GST can transform phases with electrical pulses or light pulses. People use significantly different electrical/optical properties in different phases to achieve data storage.

The scanning electron microscope images of our all-fiber memory cell are shown in Figs. 2(a)–2(d). The thicknesses of the GST and ITO are 120 nm and 30 nm, respectively. ITO prevents GST from being oxidized. Our all-fiber storage unit realizes optical storage by using the difference in reflectance between a-GST and c-GST. The scheme is the same as the principle used in conventional optical storage (where reflectivity is modulated). The crystalline state (which we term "level 1") exhibits higher reflectivity than the amorphous state ("level 0") [44,45]. Therefore, we define the conversion from a-GST to c-GST (crystallization) as the "write" process and the conversion from c-GST to a-GST (amorphization) as the "erase" process; the principle of GST transformation is shown in Fig. 1. We simulate a single 10 ns, 47 mW optical pulse train (the number is 100, and the repetition rate is 1 kHz) to heat GST to 580 K (see Fig. 3) to achieve the crystallization temperature of GST (500–600 K), and the 48.5 mW optical pulse can heat GST to an amorphous state, reaching the amorphous temperature of GST (890 K) [46].

Multi-level storage requires the cell reflectivity to be programmed with higher accuracy as compared to bi-level storage. We must precisely control the crystal fraction of the active GST material to achieve the required cell reflectivity value with adequate accuracy [47]. We select a 15 μm × 15 μm square area of GST, and the area where the temperature surpasses the melting temperature of GST (890 K) is shown in dark red and denotes the final amorphous region of the memory cell after a single optical pulse train. With the increase of the pulse power, the amorphous area of GST gradually becomes more considerable. In this paper, we assume that the two states with the largest reflectivity differences are completely crystalline and completely amorphous. We define the amorphous ratio of the fully crystallized state as "0" and the amorphous ratio of "1" when the dark red region is the largest. We can obtain the amorphous area of GST by taking boundary points through

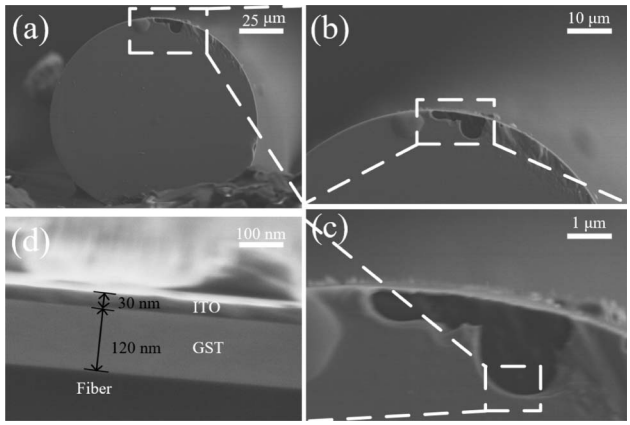

Fig. 2. Scanning electron microscope (SEM) images of the all-fiber memory cell. (a) The SEM image of GST and ITO on the optical fiber end face; the optical fiber diameter is 125 μm. (b)–(d) The fiber end face has two layers of film structure (GST and ITO), and the thickness of GST and ITO is 120 nm and 30 nm, respectively.

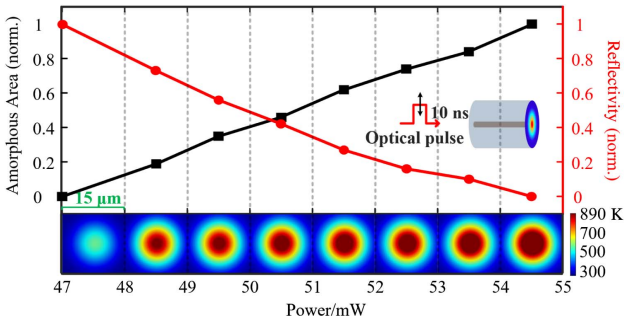

Fig. 3. Simulated temperature distribution in the GST memory cell after a 10 ns programming pulse and simulated reflectivity and crystalline fraction as functions of power. The dark red region marks the area surpassing the melting temperature of GST (890 K). The optical reflectivity of GST increases (decreases) as the crystalline fraction increases (decreases). The inset shows the model diagram of pulsed light heating GST.

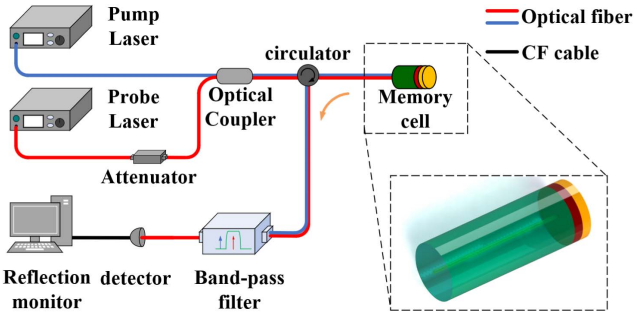

Fig. 4. Schematic of the optical measurement setup using probe/pump strategy. The pump laser (wavelength: $\lambda_1 = 1550$ nm) and the probe laser in the CW mode (wavelength: $\lambda_2 = 1530$ nm) are guided in/out of the memory cell. The output signal is filtered by a bandpass filter (BPF), connecting to a computer (PC) that monitors the reflectivity of the fiber memory at all times. The inset shows the rendered 3D picture of an all-fiber memory cell.

simulation software. The permittivity of partially amorphous GST can be calculated from effective permittivity approximated by an effective-medium theory [48,49]:

$$\frac{\varepsilon(p)-1}{\varepsilon(p)+2} = p \times \frac{\varepsilon_a - 1}{\varepsilon_a + 2} + (1-p) \times \frac{\varepsilon_c - 1}{\varepsilon_c + 2}, \quad (1)$$

where ε_c and ε_a are the complex permittivity of c-GST and a-GST, respectively, and p is the degree of amorphization (ratio of partially amorphous area to completely amorphous area). Moreover, the permittivity can be calculated from the refractive indices of GST by $\varepsilon^{0.5} = n + i\kappa$, where n is the real part of the refractive index of GST, and κ is the imaginary part of the refractive index of GST. Thus, the different levels of amorphization of GST lead to various values of $\varepsilon(p)$, leading to different levels of reflectivity. Figure 3 shows the reflectance of GST with different amorphous proportions, which is normalized. The simulated results indicate that the reflectance is inversely proportional to the amorphous area of GST.

3. RESULTS AND DISCUSSION

Our all-fiber memory device consists of a GST thin film passivated with a layer to prevent GST from oxidizing (ITO) and a single-mode fiber. GST is deposited on the end face of the fiber by radio frequency (RF) sputtering (50 W RF power, 30 mTorr Ar atmosphere, and 9×10^{-4} Torr base pressure), and ITO is deposited by direct current (RF) sputtering (10 W power, 15 mTorr Ar atmosphere, and 9×10^{-4} Torr base pressure). All depositions are performed at room temperature.

We use a pulsed laser (wavelength: $\lambda_1 = 1550$ nm) to switch the state of the fiber memory, and we use a continuous-wave laser (wavelength: $\lambda_2 = 1530$ nm) to monitor the optical reflection (optical memory level). The optical setup in the experimental measurements is sketched in Fig. 4. The probe signal is attenuated by an attenuator (0.2 mW) to reduce potential drifts caused by the thermal-optical effect of GST. Then the two optical beams are injected into the all-fiber memory cell through the optical coupler and the circulator (CIR). The fiber reflects the pump pulses and the probe signal. The optical pulses are filtered by the bandpass filter. A data acquisition card connects a photodetector to a computer to monitor the all-fiber memory's reflection in real time.

The optical reflection of the a-GST is defined as the baseline; the pulse train (the number is 100 and the repetition rate is 1 kHz) with a fixed width of 10 ns and different peak power (P_i, $i = 2, 3, 4, 5, 6, 7, 8$) can switch the state of fiber memory. The reflectivity change is defined as $\Delta R_i = R_i - R_1$, where R_i ($i = 2, 3, 4, 5, 6, 7, 8$) is the final reflectivity after laser irradiation, and R_1 is the initial reflectivity before laser irradiation (lower reflection). The relative reflectivity change is expressed as $(\Delta R_i/R_1) \times 100\%$, and the different relative reflectivity presents the different levels. We define the P_8 level as entirely crystalline and the P_1 level as entirely amorphous; other levels are partly crystalline or partly amorphous.

Here the powers of different optical pump pulses are $P_1 = 54.5$ mW, $P_i = 53.5$, 52.5, 51.5, 50.5, 49.5, 48.5, 47 mW ($i = 2, 3, 4, 5, 6, 7, 8$) in the experiment, and the optical power increase from P_8 to P_7 is more than the others, which can make the result of the experiment have a better linear relationship. The corresponding energies are 54.5, 53.5, 52.5, 51.5, 50.5, 49.5, 48.5, and 47.0 nJ.

Levels 1 to 8 are sequentially achieved by decreasing the power from P_1 to P_8. The PAM switching can also work vice versa for the amorphization. For example, levels 8 down to 1 are sequentially achieved by increasing the power from P_8 to P_1 [Fig. 5(a)]. Importantly, we can use a pulse sequence with a power of P_i to switch to any energy level i, and this switch does not consider the state of GST. Moreover, the reflectivity contrast is about 38% between levels 1 and 8. The result demonstrates that our all-fiber memory cell has good reversibility and high contrast in optical reflection. Figure 5(c) also demonstrates that the same level has the same corresponding P_1 and P_i, and each level is not affected by the previous state. It implies that every level can be accessed from all others, with accurate reflection levels and remarkable repeatability.

Level 6, for example, can be achieved from the level 1, 5, or 8 with the power of pump pulse of P_6. Due to our unique fiber reflection structure (different from the waveguide structure), the impact of a pulse sequence on GST may be divided into

two parts. The first part of the energy heats the GST into a crystalline state (initialization process). During this conversion process, the absorption coefficient k of GST gradually increases, so the energy acting on GST gradually will increase. The power is large enough to make the GST amorphized, so the subsequent pulses gradually accumulate to convert the GST to the amorphous state. The final switching level depends on the power of the light pulse [50]; the higher the optical pulse power, the greater the degree of amorphization of GST, resulting in lower reflectivity. Hence, the level and power have a "one-to-one" relationship between values, so the all-fiber memory can realize arbitrary switching by using the power of the optical pump pulse (P_i) corresponding to this level. When the initial complex refractive index of the GST is relatively large, the energy of the initial pulses is easier to act on, so the number of pulses will be small. Conversely, when the initial complex refractive index is small, more pulses are required to act on the GST. Due to the state's difference after initialization, the same state may still be achieved even if the number of accumulated pulses is different. From Figs. 5(a) and 5(c), we can see that our multi-level switching has a small drifting.

We repeatedly switch GST states between levels 1 and 8 to further describe the storage performance. Figure 5(b) shows the result of repeated switching over 40 cycles, demonstrating that the all-optical data storage on the fiber end face has high repeatability. PCMs have operation cycles up to 10^{11} and stay in the state for many years until sufficiently enormous energy is applied to PCMs [51]. We repeat the same series of pulses 10 times and plot a histogram of the error between the target reflectivity and actual reflectivity [see Fig. 5(d)]. It can be seen that the energy drift error of our device is within ±1.5%. We also have supplemented the experiment for investigating the thermo-optical effect of GST, as shown in Fig. 5(e). It can be seen for a single pulse that the response time of the amorphization process is 158 ns, and the response time of the crystallization process is 145 ns.

We can use memory cells to manufacture all-fiber logic gates ("AND," "OR"), which can meet the requirement of next-generation optical networks [52]. We name the present optical memory as "memlogic," which is short for memory logic with both nonvolatile configurations of logic functions and nonvolatile logic output results [53].

Optical pulses of the power (P_8 and P_1) corresponding to the entirely crystalline state (level 8) and entirely amorphous state (level 1) are used as the logic input "1" and the logic input "0" (the two logic inputs have the same pulse width $W = 10$ ns); the enormous optical contrast makes the two logic inputs more easily distinguished. As a result, the logic output has a higher contrast ratio when carrying out logic operations. Here, we define the normalized reflection (NR) of the two input pulses passing through two memlogic units as the logic output.

Figure 6(a) shows the logic operation principle of typical memlogic cells. First, as shown in Fig. 6(a), we connect two memlogic cells in series to perform the "AND" logic operation. Next, we connect two memlogic cells in parallel and combine

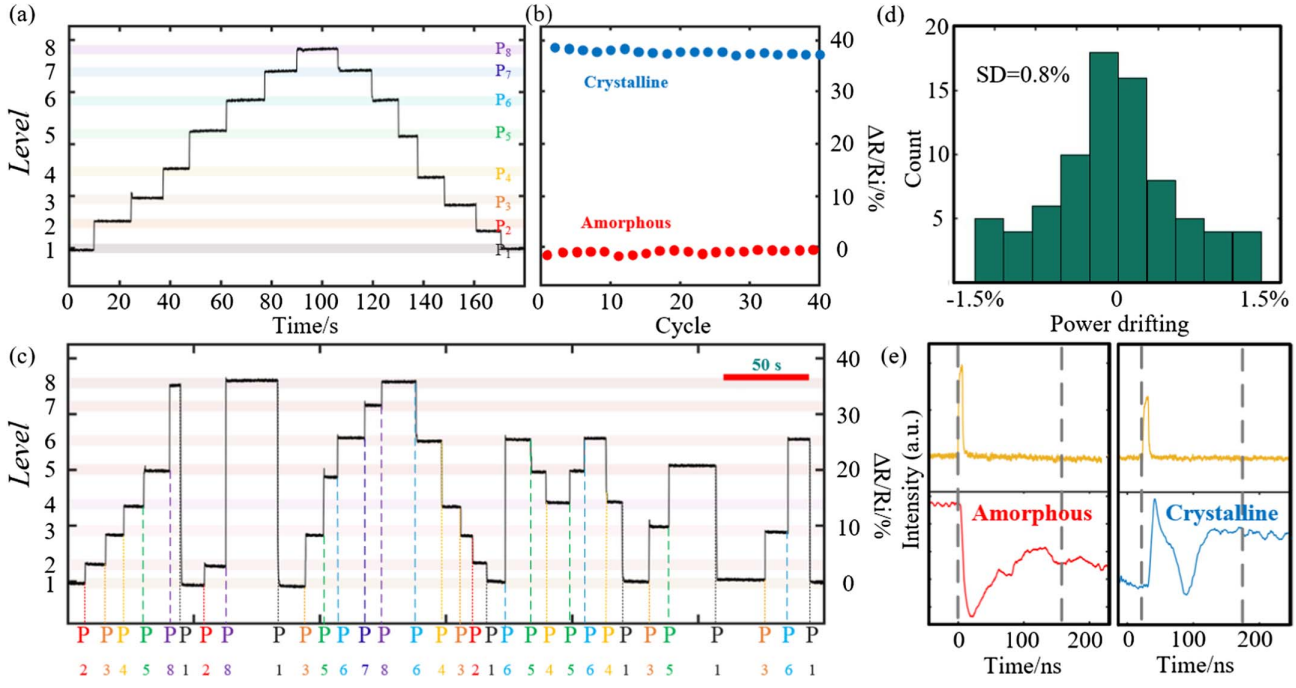

Fig. 5. Measurements of multi-level operation using the PAM programming technique. (a) Experimental demonstration of eight different levels in the all-fiber device with the relative change in reflection ($\Delta R/R_i$) recorded. A single pulse train with width $W = 10$ ns is implemented to switch the photonic memory, and each level is reached by a determined optical power, from 54.5 to 47 mW. $P_1 = 54.5$ mW, $P_i = 53.5, 52.5, 51.5, 50.5, 49.5, 48.5, 47$ mW ($i = 2, 3, 4, 5, 6, 7, 8$). (b) Multiple repetitions of the same switching cycle (levels 8 and 1) as in (a). Moreover, the 40 cycles verified a confidence interval of ±2.2%. (c) Accessing same levels but in random order featuring intra-level switching. Each level can also be independently reached and erased, with very accurate control of the reflection levels and remarkable repeatability. (d) Histogram plots of the difference between the desired reflectivity level and the actual reflectivity level. (e) Response time of a single pulse amorphization and crystallization; the time is 158 ns and 145 ns, respectively (the pulse width is 10 ns).

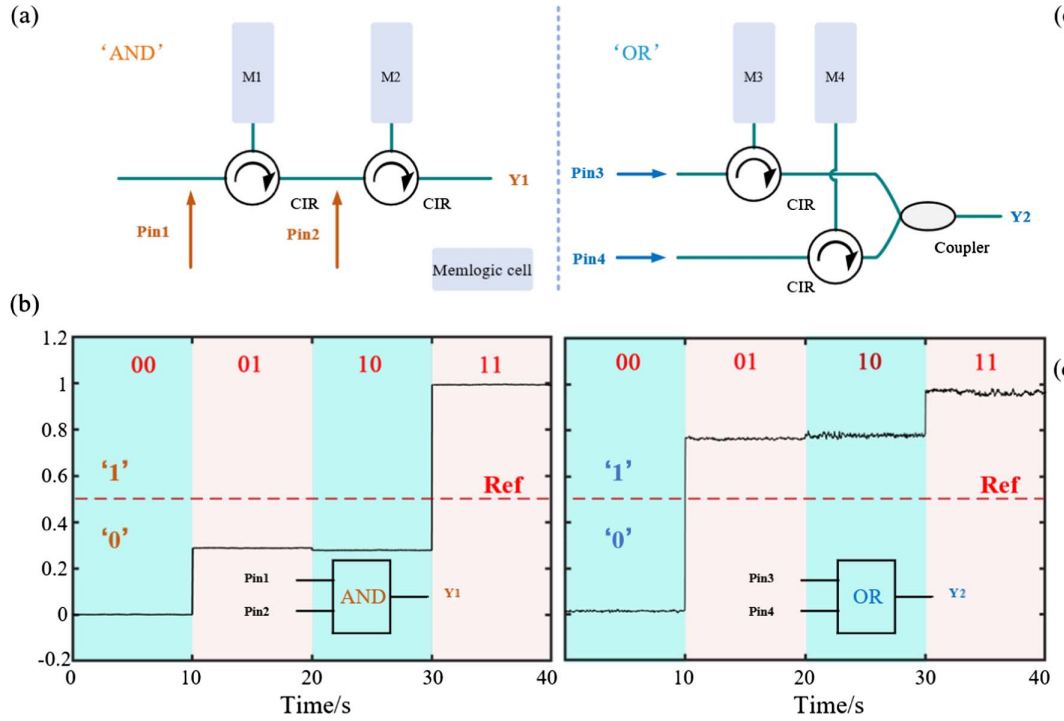

(c)

AND			
Input		Output	
Pin1	Pin2	Y1	NR
0	0	0	0.00
0	1	0	0.29
1	0	0	0.28
1	1	1	0.99

(d)

OR			
Input		Output	
Pin3	Pin4	Y2	NR
0	0	0	0.01
0	1	1	0.76
1	0	1	0.78
1	1	1	0.96

Fig. 6. Results of logical operation experiment. (a) Schematic of an optical logic device based on the fiber memory with two signal inputs Pin1 and Pin2 (Pin3 and Pin4). The "AND" gate is realized by using two storage logic units in series, and the "OR" gate is realized by combining the output signals of the two units with the coupler after two storage logic operation units are connected in parallel. (b) The normalized reflectivity outputs of the memlogic with different input combinations. The output is defined as logic "1" above the reference value. Moreover, the diagram on the left is the relationship between the input and output of the "AND" gate, and the diagram on the right is the relationship between the input and output of the "OR" gate. (c), (d) The truth table of the basic logic "AND," "OR" calculation. Output at four different combinations of input states: ("1," "1"); ("1," "0"); ("0," "1"); and ("0," "0").

two outputs with a coupler to achieve the "OR" logic operation. Each memlogic unit must be connected to a CIR because our all-fiber memory measures the reflection of the fiber. The reflectivities of two series memlogic units are defined as R_{in1}, R_{in2}, and the reflectivities of "OR" gate memlogic units are defined as R_{in3}, R_{in4}, respectively. According to the series and parallel characteristics of two memlogic units, the value of the reflectivity output after series (R_s) and parallel (R_p) connections can be expressed as $R_s = R_{in1} \times R_{in2}$; $R_p = R_{in3} + R_{in4}$. The input information is stored in the memlogic cell and is read by a continuous wavelength light. We conduct an optical erasing process with both memlogic cells to ensure they are in the amorphous state before performing the logic calculation. We take the "AND" gate in series as an example. We use two independent optical pulses as optical inputs (Pin1, Pin2), and the two pulses of fixed width (10 ns) are used to program digital inputs "0," "1," corresponding to pulse amplitudes of 54.5 mW, 47 mW, respectively, and are applied to memlogic cells. As shown in Fig. 6(b), we can obtain distinct NR values with different digit combinations of Pin1 and Pin2 (Pin3 and Pin4). We compared the value of NR with the reference value of 0.5 (red line); the logic output (Y1 and Y2) of the optical memory can be either "0" or "1" (below and above the reference line). When the inputs are "00," "01," "10," and "11", respectively, the NRs are 0.00, 0.29, 0.28, and 0.99 in the logic device of the "AND" gate, and the outputs are 0.01, 0.76, 0.78, and 0.96 in the logic device of the "OR" gate. We set the reference line to 0.5. Thus, the logic "AND" and logic "OR" outputs are "0," "0," "0," "1," and "0," "1," "1," "1", respectively. The truth tables of the memlogic cells are shown as Figs. 6(c) and 6(d), corresponding to the results of the traditional electronic "AND" and "OR" gates, respectively.

Importantly, when the logic inputs of Pin1 and Pin2 are "1," "0" or "0," "1", respectively, the values of NR are different because the reflectivity contrast is different of two memlogic cells. Moreover, the differences between the two outputs will increase because of the increasing difference in the memlogic units' reflectivity contrast. However, the final logic results are not affected by this slight difference. Finally, it is worth mentioning that we can extend our logic devices to achieve more complex optical logic functions (normalizing reflectivity, a standardized device is added after each logic gate). Therefore, our fiber memlogic cells have excellent potential in all-optical networks.

4. CONCLUSION

In summary, we have shown the demonstration of 3-bit data storage with an all-fiber memory cell. We use the PAM switching technique to realize partial crystallization of the PCM memory cell, and we can control the reflectivity in the GST layer by pulse power (~50 nJ). Furthermore, we show the

readily and directly switching ability between the multiple memory levels, with high accuracy of the readout signal and excellent repeatability. Moreover, we use the memlogic units in series and parallel to realize the essential logic operation ("AND" and "OR"), and we can recognize more complex logic operations by using more fiber optic memlogic cells.

The results are a broad and fundamental step toward a fast, low-power fiber memory for applications. The all-fiber nonvolatile multi-level memory can have applications such as neuromorphic computing and in-memory computing. The primary logic gate is expected to realize more complex logic operations. The application of the memlogic unit in optical fiber communication networks is expected to lead to a new revolution in optical fiber communication technology.

Funding. National Key Research and Development Program of China (2018YFC1503703); National Natural Science Foundation of China (61775047, 61975039); Natural Science Foundation of Heilongjiang Province of China (YQ2020F011); 111 Project (B13015); Fundamental Research Funds for Harbin Engineering University of China.

Acknowledgment. The authors thank the College of Physics and Optoelectronic Engineering of Harbin Engineering University for providing technical support under the Key Laboratory of In-fiber Integrated Optics, Ministry of Education, China.

Disclosures. The authors declare no conflicts of interest.

Data Availability. Data underlying the results presented in this paper are not publicly available at this time but may be obtained from the authors upon reasonable request.

REFERENCES

1. T. Lagkas, D. Klonidis, P. Sarigiannidis, and I. Tomkos, "5G/NGPON evolution and convergence: developing on spatial multiplexing of optical fiber links for 5G infrastructures," Fiber Integr. Opt. **39**, 4–23 (2020).
2. S. Bjorn, B. Giulio, R. Ahmad, C. Fabio, and O. Peter, "Rethinking optical transport to pave the way for 5G and the networked society," J. Lightwave Technol. **33**, 1084–1091 (2015).
3. J. S. Wey and J. W. Zhang, "Passive optical networks for 5G transport: technology and standards," J. Lightwave Technol. **37**, 2830–2837 (2019).
4. B. Lee, "Review of the present status of optical fiber sensors," Opt. Fiber Technol. **9**, 57–79 (2003).
5. D. Wang, Q. Sui, and Z. Li, "Toward universal optical performance monitoring for intelligent optical fiber communication networks," IEEE Commun. Mag. **58**, 54–59 (2020).
6. P. Iovanna, F. Cavaliere, S. Stracca, L. Giorgi, and F. Ubaldi, "5G xhaul and service convergence: transmission, switching and automation enabling technologies," J. Lightwave Technol. **38**, 2799–2806 (2020).
7. G. Wellbrock, T. Wang, and O. Ishida, "New paradigms in optical communications and networks," IEEE Commun. Mag. **51**, 22–23 (2013).
8. M. Naghshvarianjahromi, S. Kumar, and M. J. Deen, "Smart long-haul fiber optic communication systems using brain-like intelligence," in *16th Canadian Workshop on Information Theory (CWIT)* (2019), pp. 1–6.
9. N. Pleros, D. Apostolopoulos, D. Petrantonakis, C. Stamatiadis, and H. Avramopoulos, "Optical static RAM cell," IEEE Photonics Technol. Lett. **21**, 73–75 (2009).
10. D. Fitsios, C. Vagionas, G. T. Kanellos, A. Miliou, and N. Pleros, "Dual-wavelength bit input optical RAM with three SOA-XGM switches," IEEE Photonics Technol. Lett. **24**, 1142–1144 (2012).
11. C. Vagionas, D. Fitsios, G. T. Kanellos, N. Pleros, and A. Miliou, "Optical RAM and flip-flops using bit-input wavelength diversity and SOA-XGM switches," J. Lightwave Technol. **30**, 3003–3009 (2012).
12. M. Hill, H. Dorren, T. D. Vries, X. Leijtens, J. D. Besten, B. Smalbrugge, Y. Oei, H. Binsma, G. Khoe, and M. Smit, "A fast low-power optical memory based on coupled micro-ring lasers," Nature **432**, 206–209 (2004).
13. A. Trita, G. Mezõsi, M. Sorel, and G. Giuliani, "All-optical toggle flip-flop based on monolithic semiconductor ring laser," IEEE Photonics Technol. Lett. **26**, 96–99 (2014).
14. P. Bakopoulos, K. Vyrsokinos, D. Fitsios, T. Alexoudi, D. Apostolopoulos, H. Avramopoulos, A. Miliou, and N. Pleros, "All-optical T-flip-flop using a single SOA-MZI-based latching element," IEEE Photonics Technol. Lett. **24**, 748–750 (2012).
15. Y. Naito, S. Shimizu, T. Kato, K. Kobayashi, and H. Uenohara, "Investigation of all-optical latching operation of a monolithically integrated SOA-MZI with a feedback loop," Opt. Express **20**, B339–B349 (2012).
16. C. H. Chen, S. Matsuo, K. Nozaki, A. Shinya, and M. Notomi, "All-optical memory based on injection-locking bistability in photonic crystal lasers," Opt. Express **19**, 3387–3395 (2011).
17. J. Sakaguchi, T. Katayama, and H. Kawaguchi, "All-optical memory operation of 980-nm polarization bistable VCSEL for 20-Gb/s PRBS RZ and 40-Gb/s NRZ data signals," Opt. Express **18**, 12362–12370 (2010).
18. T. Katayama, T. Ooi, and H. Kawaguchi, "Experimental demonstration of multi-bit optical buffer memory using 1.55-μm polarization bistable vertical-cavity surface-emitting lasers," IEEE J. Quantum Electron. **45**, 1495–1504 (2009).
19. D. Fitsios, T. Alexoudi, A. Bazin, P. Monnier, R. Raj, A. Miliou, G. T. Kanellos, N. Pleros, and F. Raineri, "Ultra-compact III–V-on-Si photonic crystal memory for flip-flop operation at 5 Gb/s," Opt. Express **24**, 4270–4277 (2016).
20. T. Alexoudi, D. Fitsios, G. Kanellos, A. Miliou, A. Bazin, R. Raj, F. Raineri, N. Pleros, and P. Monnier, "III-V-on-Si photonic crystal nanocavity laser technology for optical static random access memories," IEEE J. Sel. Top. Quantum Electron. **22**, 4901410 (2016).
21. D. K. Loke, J. M. Skelton, T. H. Lee, R. Zhao, T. C. Chong, and S. R. Elliott, "Ultrafast nanoscale phase-change memory enabled by single-pulse conditioning," ACS Appl. Mater. Interfaces **10**, 41855–41860 (2018).
22. T. Matsunaga, J. Akola, S. Kohara, T. Honma, K. Kobayashi, E. Ikenaga, R. O. Jones, N. Yamada, M. Takata, and R. Kojima, "From local structure to nanosecond recrystallization dynamics in AgInSbTe phase-change materials," Nat. Mater. **10**, 34–1129 (2011).
23. M. Salinga, B. Kersting, I. Ronneberger, V. P. Jonnalagadda, X. T. Vu, M. L. Gallo, I. Giannopoulos, O. C. Mirédin, R. Mazzarello, and A. Sebastian, "Monatomic phase change memory," Nat. Mater. **17**, 681–685 (2018).
24. W. Zhang and E. Ma, "Single-element glass to record data," Nat. Mater. **17**, 654–655 (2018).
25. F. Rao, K. Ding, Y. Zhou, Y. Zheng, M. Xia, S. Lv, Z. Song, S. Feng, I. Ronneberger, and R. Mazzarello, "Reducing the stochasticity of crystal nucleation to enable subnanosecond memory writing," Science **358**, 1423–1427 (2017).
26. G. M. Zewdie, Y. X. Zhou, L. Sun, F. Rao, V. L. Deringer, R. Mazzarello, and W. Zhang, "Chemical design principles for cache-type Sc-Sb-Te phase-change memory materials," Chem. Mater. **31**, 4008–4015 (2019).
27. M. S. Arjunan, N. Saxena, A. Mondal, T. Dixit, and A. Manivannan, "High-stability and low-noise multi-level switching in In_3SbTe_2 material for phase change photonic memory applications," Phys. Status Solidi Rapid Res. Lett. **15**, 2000354 (2021).
28. C. Zou, J. Zheng, C. Chang, A. Majumdar, and L. Y. Lin, "Nonvolatile rewritable photomemory arrays based on reversible phase-change

perovskite for optical information storage," Adv. Opt. Mater. **7**, 1900558 (2019).
29. W. H. P. Pernice and H. Bhaskaran, "Photonic nonvolatile memories using phase change materials," Appl. Phys. Lett. **101**, 171101 (2012).
30. C. Ríos, M. Stegmaier, P. Hosseini, D. Wang, T. Scherer, C. D. Wright, H. Bhaskaran, and W. H. P. Pernice, "Integrated all-photonic nonvolatile multi-level memory," Nat. Photonics **9**, 725–732 (2015).
31. E. Gemo, S. G. C. Carrillo, C. R. D. Galarreta, A. Baldycheva, and C. D. Wright, "Plasmonically-enhanced all-optical integrated phase-change memory," Opt. Express **27**, 24724–24737 (2019).
32. X. Li, N. Youngblood, C. Ríos, Z. G. Cheng, C. D. Wright, W. H. P. Pernice, and H. Bhaskaran, "Fast and reliable storage using a 5 bit, nonvolatile photonic memory cell," Optica **6**, 1–6 (2019).
33. Y. Zhang, J. B. Chou, J. Li, H. Li, Q. Du, A. Yadav, S. Zhou, M. Y. Shalaginov, Z. Fang, and H. Zhong, "Broadband transparent optical phase change materials for high-performance nonvolatile photonics," Nat. Commun. **10**, 1 (2019).
34. M. S. Arjunan, A. Mondal, A. Das, K. V. Adarsh, and A. Manivannan, "Multi-level accumulative switching processes in growth-dominated AgInSbTe phase change material," Opt. Lett. **44**, 3134–3137 (2019).
35. A. M. Sreekrishnan, A. Mondal, S. Durai, K. V. Adarsh, and A. Manivannan, "Impact of crystallization process in multi-level optical switching in $Ge_2Sb_2Te_5$ and $Ag_5In_5Sb_{60}Te_{30}$ phase-change materials," J. Phys. D **53**, 495303 (2020).
36. Z. G. Cheng, C. Ríos, N. Youngblood, C. D. Wright, W. H. P. Pernice, and H. Bhaskaran, "Device-level photonic memories and logic applications using phase-change materials," Adv. Mater. **30**, 1802435 (2018).
37. R. Marchetti, C. Lacava, L. Carroll, K. Gradkowski, and P. Minzioni, "Coupling strategies for silicon photonics integrated chips," Photon. Res. **7**, 201–239 (2019).
38. H. J. S. Dorren, M. T. Hill, Y. Liu, N. Calabretta, A. Srivatsa, F. M. Huijskens, H. D. Waardt, and G. D. Khoe, "Optical packet switching and buffering by using all-optical signal processing methods," J. Lightwave Technol. **21**, 2–12 (2003).
39. G. C. Carrillo, G. R. Nash, H. Hayat, J. C. Martin, K. Maciej, H. Bhaskaran, and C. D. Wright, "Design of practicable phase-change metadevices for near-infrared absorber and modulator applications," Opt. Express **24**, 13563–13573 (2016).
40. D. Lencer, M. Salinga, and M. Wuttig, "Design rules for phase-change materials in data storage applications," Adv. Mater. **23**, 2030–2058 (2011).
41. C. Ríos, N. Youngblood, Z. Cheng, M. L. Gallo, W. H. P. Pernice, C. D. Wright, A. Sebastian, and H. Bhaskaran, "In-memory computing on a photonic platform," Sci. Adv. **5**, eaau5759 (2019).
42. J. Feldmann, M. Stegmaier, N. Gruhler, C. Ríos, H. Bhaskaran, C. D. Wright, and W. H. P. Pernice, "Calculating with light using a chip-scale all-optical abacus," Nat. Commun. **8**, 1256 (2017).
43. S. Abdollahramezani, O. Hemmatyar, H. Taghinejad, A. Krasnok, and A. Adibi, "Tunable nanophotonics enabled by chalcogenide phase-change materials," Nanophotonics **9**, 1189–1241 (2020).
44. L. Wang, L. Tu, and J. Wen, "Application of phase-change materials in memory taxonomy," Sci. Technol. Adv. Mater. **18**, 406–429 (2017).
45. J. Siegel, A. Schropp, J. Solis, C. N. Afonso, and M. Wuttig, "Rewritable phase-change optical recording in $Ge_2Sb_2Te_5$ films induced by picosecond laser pulses," Appl. Phys. Lett. **84**, 2250–2252 (2004).
46. N. Yamada, E. Ohno, K. Nishiuchi, N. Akahira, and M. Takao, "Rapid-phase transitions of GeTe-Sb_2Te_3 pseudobinary amorphous thin films for an optical disk memory," J. Appl. Phys. **69**, 2849–2856 (1991).
47. E. Kuramochi and M. Notomi, "Phase-change memory," Nat. Photonics **9**, 712–714 (2015).
48. Y. G. Chen, X. Li, Y. Sonnefraud, I. F. D. Antonio, X. G. Luo, M. H. Hong, and S. A. Maier, "Engineering the phase front of light with phase-change material based planar lenses," Sci. Rep. **5**, 8660 (2015).
49. N. V. Voshchinnikov, G. Videen, and T. Henning, "Effective medium theories for irregular fluffy structures: aggregation of small particles," Appl. Opt. **46**, 4065–4072 (2007).
50. C. Rios, M. Stegmaier, Z. G. Cheng, N. Youngblood, C. D. Wright, W. H. P. Pernice, and H. Bhaskaran, "Controlled switching of phase-change materials by evanescent-field coupling in integrated photonics," Opt. Mater. Express **8**, 2455–2470 (2018).
51. M. Stegmaier, C. Rios, P. Hosseini, C. D. Wright, H. Bhaskaran, and W. H. P. Pernice, "All-photonic nonvolatile memory cells using phase-change materials," in *IEEE Photonics Conference* (2015), pp. 484–485.
52. J. Y. Tian, H. Luo, Y. Q. Yang, F. Ding, Y. R. Qu, D. Zhao, M. Qiu, and S. I. Bozhevolnyi, "Active control of anapole states by structuring the phase-change alloy $Ge_2Sb_2Te_5$," Nat. Commun. **10**, 396 (2019).
53. H. W. Tan, G. Liu, H. L. Yang, X. H. Yi, L. Pan, J. Shang, S. B. Long, M. Liu, Y. H. Wu, and R. W. Li, "Light-gated memristor with integrated logic and memory functions," ACS Nano **11**, 11298–11305 (2017).